Oxygen vacancy-rich Fe_3O_4 enriched P–Fe_2TiO_5 sites generated by Na incorporation and Ni–P deposition for accelerated electrocatalytic OER

Revathy B. Nair[a], A. Anantha Krishnan[b], Aneesh Kumar M. A.[b], Sreehari Harikumar[b], Meera B[c], Vidhya C.[c], M. Ameen Sha[c], Logudurai Radhakrishnan[d]*, Sajith Kurian[a]*, P. S. Arun[b]*

a. *Department of Chemistry, Mar Ivanios College (Affiliated to University of Kerala), Nalanchira, Thiruvanathapuram, Kerala - 695015, India. E-mail: sajith.kurian@mic.ac.in*
b. *Department of Chemistry, St. John's College (Affiliated to University of Kerala), Anchal, Kollam, Kerala - 691306, India. E-mail: arunps@stjohns.ac.in*
c. *Department of Chemistry, University of Kerala, Kariavattom Campus, Thiruvanathapuram, Kerala - 695581, India. E-mail: shaalameen@gmail.com*
d. *Division of Chemistry, SRM Institute of Science and Technology – Tiruchirappalli - 621105, Tamil Nādu, India. Email: logudurr@srmist.edu.in*

Material characterisation

Fe–FT, Na–Fe–FT (powder samples), Fe–FT/NiP and Na–Fe–FT/NiP electrodes were characterized using various techniques. Surface topography, structure, elemental analysis and mapping the chemical composition were analysed by FE–SEM and EDAX using a Carl Zeiss–Sigma 300 scanning electron microscope. Crystallographic information of all the samples were studied by X–Ray Diffraction (XRD) analysis using a Bruker D8 Advance twin–twin spectrometer. X–Ray Photoelectron Spectroscopy (XPS) analysis was performed using a Thermo Scientific ECSALAB Xi+ photoelectron spectrometer, which employed an Al K–α X–ray source with an energy of 1486.6 eV. The binding energy obtained from this analysis was calibrated using carbon 1s (284.6 eV) as a reference.

Electrochemical characterization and OER performance.

The electrochemical performance of the fabricated electrodes toward the Oxygen Evolution Reaction (OER) was evaluated using a conventional three–electrode system. In this setup, the fabricated electrode served as the working electrode, while a Pt mesh (5 cm^2) and HgO/Hg electrode were employed as the counter and reference electrode, respectively, all connected to an electrochemical workstation (CH16041E). Electrochemical Impedance Spectroscopy (EIS) was carried out in 1 M NaOH at the Open Circuit Potential (OCP), covering a frequency range from 1 Hz to 100 kHz to analyze charge-transfer resistance and interfacial behaviour. The Electrochemically Active Surface Area (ECSA) of the electrodes was estimated using Cyclic Voltammetry (CV) measurements at non-faradaic region, recorded at different scan rates. The OER activity of the developed electrodes was further assessed using Linear Sweep Voltammetry (LSV) in 1 M NaOH, at a scan rate of 10 mV s^{-1} within a scanning window from 1.2 V to 1.7 V versus the Reversible Hydrogen Electrode (RHE). The kinetics of the OER reactions were estimated from Tafel plots obtained using short term chronoamperometric analysis (CA). The electrochemical stability of the electrodes during OER was verified by comparing the LSV curves recorded before and after 1000 consecutive CV cycles.

Photocatalytic HER performance

The photocatalytic performance of the developed electrodes was evaluated under direct sunlight. A 2 cm^2 surface area of the electrode was exposed to sunlight. The developed electrodes were carefully placed inside a 70 mL round-bottom flask containing a 25% v/v methanol/water mixture, and the flask was sealed with a septum. Nitrogen gas was purged for 45 minutes to deaerate the solution before

the activity measurements. The developed electrodes were irradiated for 5 hours. The generated H_2 gas was periodically collected and analyzed using a gas chromatograph (PerkinElmer Clarus 590 GC) equipped with a thermal conductivity detector at 473 K. All the photocatalytic HER reactions were repeated at least four times using different electrode batches, with results within a 4% error margin. The electrode with the highest performance was tested for reusability under the same experimental conditions. Nitrogen gas was purged after each cycle to remove hydrogen gas generated during the previous cycle.

EDX spectra and mapping

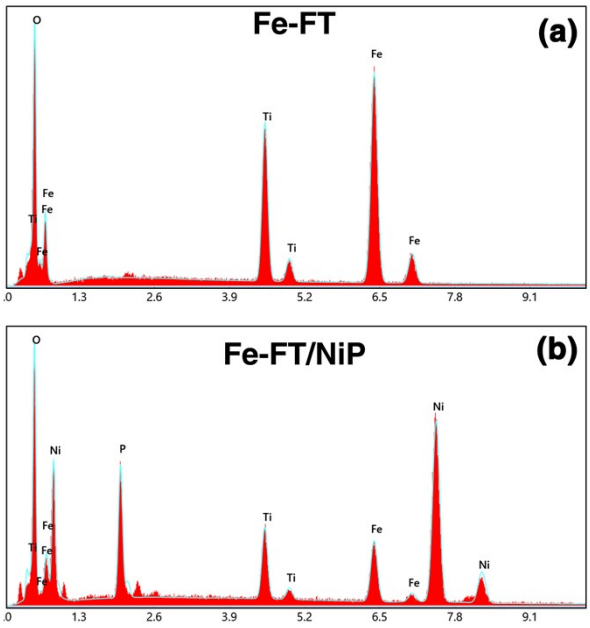

Fig. S1. Comparison of EDX spectra of Fe–FT powder and Fe–FT/NiP electrode.

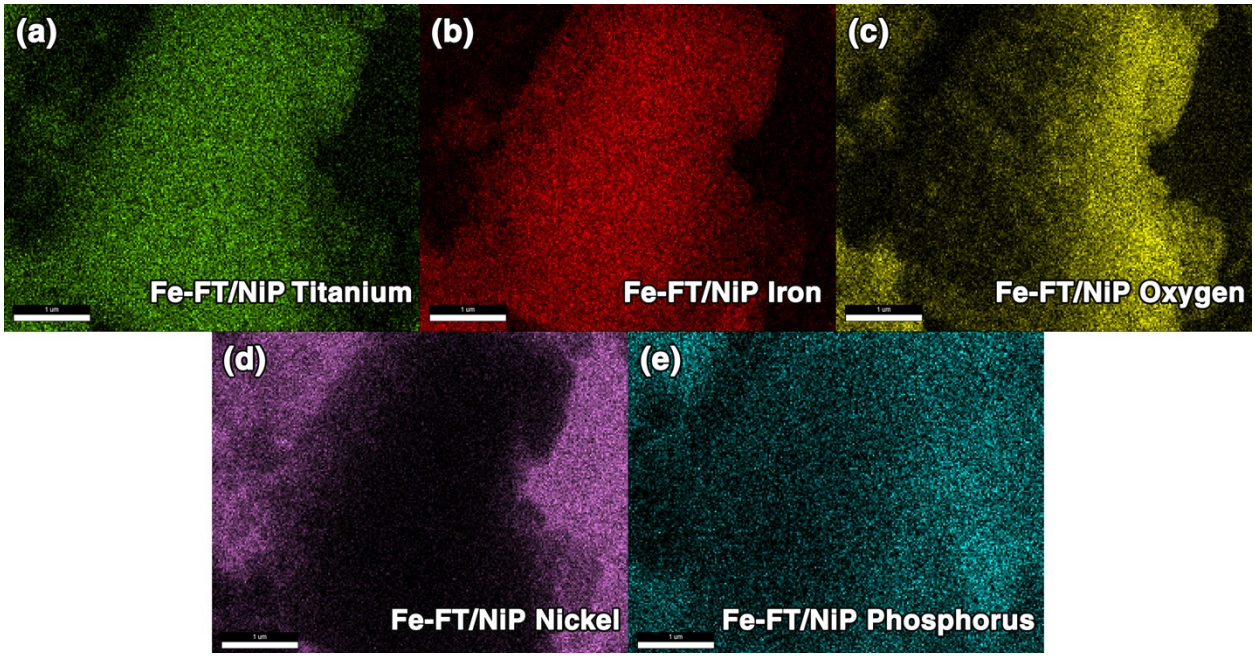

Fig. S2. EDX mapping of various elements present in Fe–FT/NiP electrode

Electrocatalytic analysis

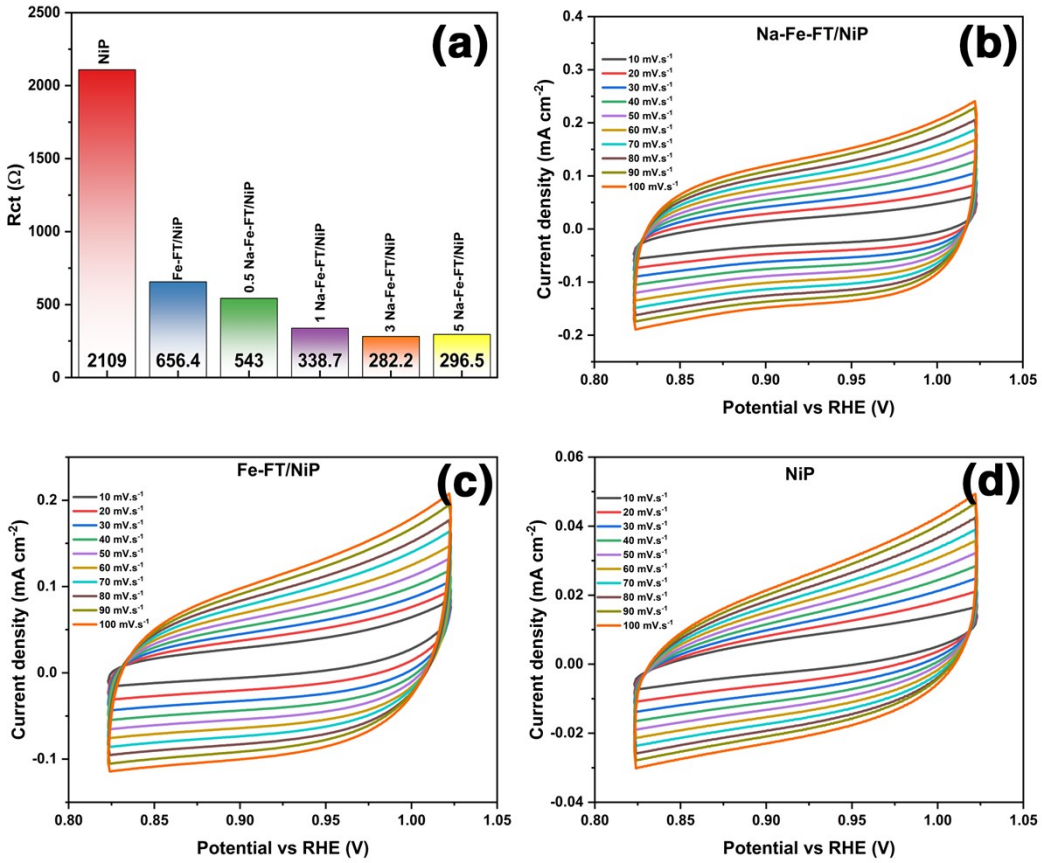

Fig. S3. (a). Column graph tabulating the R_{ct} values of all electrodes (b-d) The CV graph of Na-Fe-FT/NiP, Fe-FT/NiP and NiP electrode at different scan rates taken at the non-faradaic region.

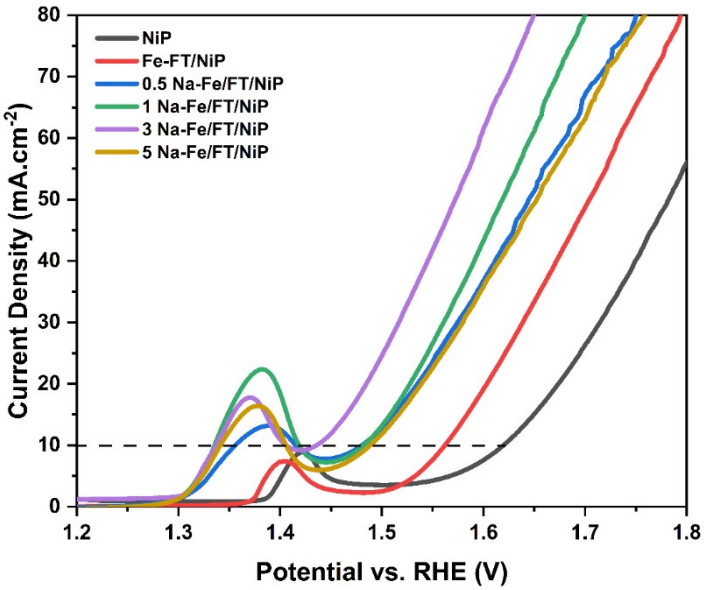

Fig. S4. LSV of all Na-Fe-FT/NiP electrodes along with NiP and Fe-FT/NiP

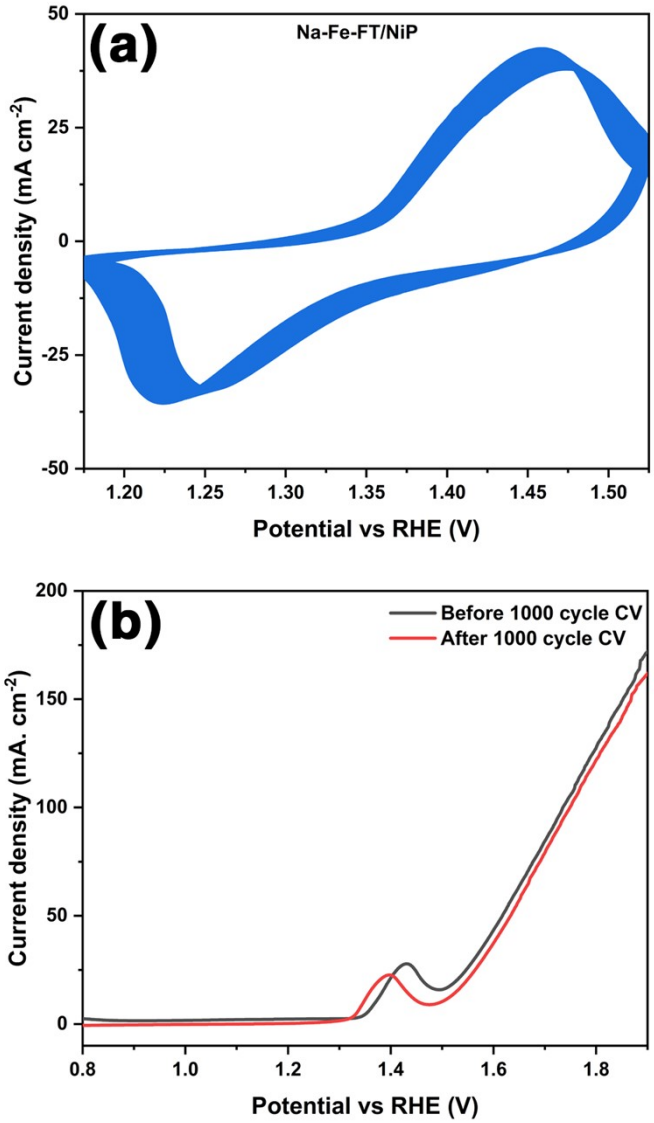

Fig. S5. (a). 1000 CV cycles of Na-Fe-FT/NiP electrode, (b) LSV taken before and after 1000 CV cycles.

Comparison to other recently published works

Table S1. Comparison of electrocatalytic OER performance with other recent publications

Sl. No.	Catalyst	Overpotential (mV)	Tafel Slope (mV dec^{-1})	Reference
1.	$Ni_{2.5}Fe_{2.5}$-P/$Ti_3C_2T_x$	290 mV@ 10 mA cm^{-2}	72.3 mV dec^{-1}	[1]
2.	NiS_2/Ti_3CNCl_2	297 mV@ 10 mA cm^{-2}	109.6 mV dec^{-1}	[2]
3.	Fe_3O_4@NiFe-LDH/$MnCO_3$	230 mV at 50 mA cm^{-2}	73.1 mV dec^{-1}	[3]
4.	Co:α-Fe_2O_3/γ-Fe_2O_3	297 mV @ 10 mA cm^{-2}	56.67 mV dec^{-1}	[4]
5.	0.3Fe-$NiCo_{1.7}O_4$/NiO@P-rGO	293 mV @ 10 mA cm^{-2}	61.55 mV dec^{-1}	[5]
6.	CoFe LDH on $Ti_3C_2T_x$ MXene	301 mV @ 10 mA cm^{-2}	43 mV dec^{-1}	[6]
7.	MXene@TiO_2/FeP	240 mV @ 10 mA cm^{-2}	74.55 mV dec^{-1}	[7]
8.	commercial RuO_2	293 mV@ 10 mA cm^{-2}	96.33 mV dec^{-1}	[7]
9.	FeP_4@TiO_2	400-450 mV@ 10 mA cm^{-2}	90 mV dec^{-1}	[8]
	Ni_2P/FeP_4@TiO_2	260 mV@ 10 mA cm^{-2}	55 mV dec^{-1}	
10.	Ti-doped NiCo-LDH/NF	319mV @50 mA cm^{-2}	117 mV dec^{-1}	[9]
11.	TiO_2/S-PANI	1213 mV@ 0.1 mA cm^{-2}	273 mV dec^{-1}	[10]
	FeOOH/S-PANI	416 mV @ 0.1 mA cm^{-2}	68-100 mV dec^{-1}	
12.	Fe_3O_4	497 mV@ 10 mA cm^{-2}	101 mV dec^{-1}	[11]
13.	Ir-black@Fe_3O_4	290 mV@ 10 mA cm^{-2}	60 mV dec^{-1}	[11]

14.	Fe_3O_4/IF	370.6 mV@ 10 mA cm^{-2}	101 mV dec^{-1}	[12]
	22%Co–Fe_3O_4/IF	260.6 mV@10 mA cm^{-2}	72.31 mV dec^{-1}	
15.	**Na-Fe-FT/NiP**	**249 mV**@10 mA cm^{-2}	**79 mV dec^{-1}**	**Present article**

References

[1] Tan L, Wang J, Zhou S, Zhu H, Guo J, Chen Y, et al. NiFe phosphides coupled on Ti3C2Tx MXene nanosheets for high-efficiency oxygen evolution reaction in alkaline medium. J Colloid Interface Sci 2025;689:137263.

[2] Li X, Wen T, Zheng Y, Zou J, Wang H. Interfacial Ti-S bond confers NiS2/Ti3CNCl2 MXene heterojunction efficient oxygen evolution electrocatalytic performance. J Power Sources 2025;653:237772.

[3] Huang A, Xu R, Zhao D, Gao X, Chen Z. Self-driven coupling field in Fe3O4@ NiFe-LDH/MnCO3 heterojunction for electrocatalytic water oxidation at high current densities. Chem Eng J 2025:166883.

[4] Soares JPG de S, Lourenço A de A, Raimundo RA, Morales Torres MA, da Silva RB, Menezes de Oliveira AL, et al. Electrocatalytic Oxygen Evolution by Cobalt-Containing Fe2O3-Based Nanoparticles and Nanocomposites. ACS Appl Nano Mater 2025.

[5] Sarkar S, Chaubey P, Sharma PK. Inverse spinel Fe-NiCo2O4/NiO nanocomposite supported on defect-rich P-rGO sheets for enhanced OER activity. J Alloys Compd 2025;1010:177856.

[6] Sheng J, Kang J, Jiang P, Meinander K, Hong X, Jiang H, et al. Guided heterostructure growth of CoFe LDH on Ti3C2Tx MXene for durably high oxygen evolution activity. Small 2025;21:2404927.

[7] Su H, Zeng X, Gui L, Zhao H, Zhang X. High-efficiency photoelectrocatalytic oxygen evolution reaction enabled by MXene-derived TiO 2 coupled with FeP nanoparticles. J Mater Chem A 2025.

[8] Tian S, Li Z, Wang H, Du X, Liu G, Li J. Phosphorus solvation induced deep reconstruction of phosphorus-doped nickel-iron oxyhydroxides towards efficient oxygen evolution reaction. Chem Eng J 2025;504:158701.

[9] Xie J, Du J, Chen P, Wang G, Zhang J, Yang X, et al. A facile route of Ti decoration for modulating M–O–Ti (M= Ni, Co) and oxygen vacancies on NiCo-LDH electrocatalysts for efficient oxygen evolution reaction. Ind Chem Mater 2025;3:342–52.

[10] Joy M, Bloom B, Govindaraj K, Albro JA, Vadakkayil A, Waldeck DH. Development of a spin selective electrocatalyst platform and its use to study spin-polarization and d-orbital occupancy effects in oxygen evolution reaction electrocatalysts. J Mater Chem A 2025.

[11] Jia X-Y, Chen Z, Liu M-D, Chang Y, Zhang S, Zeng F, et al. Preparation and Properties of Fe3O4-

Based Dimensionally Stable Anodes Derived by High-Temperature Sintering for Water Electrolysis. Ceram Int 2025.

[12] Liao R, Peng Z, Yang X, Liu J, Zhou J, Yu L, et al. Co-doped Fe3O4 nanosheets arrays on Fe foam as low-cost integrated electrocatalysts for efficient overall water electrolysis. Int J Hydrogen Energy 2025;116:32–9.